The Meteoritical Society

Meteoritics & Planetary Science 49, Nr 9, 1680–1697 (2014)
doi: 10.1111/maps.12219

Stardust Interstellar Preliminary Examination X: Impact speeds and directions of interstellar grains on the Stardust dust collector

Veerle J. STERKEN[1,2,†,*], Andrew J. WESTPHAL[3], Nicolas ALTOBELLI[4], Eberhard GRÜN[5], Jon K. HILLIER[6], Frank POSTBERG[6], Ralf SRAMA[7], Carlton ALLEN[8], David ANDERSON[3], Asna ANSARI[9], Saša BAJT[10], Ron S. BASTIEN[11], Nabil BASSIM[12], Hans A. BECHTEL[13], Janet BORG[14], Frank E. BRENKER[15], John BRIDGES[16], Donald E. BROWNLEE[17], Mark BURCHELL[18], Manfred BURGHAMMER[19], Anna L. BUTTERWORTH[3], Hitesh CHANGELA[20], Peter CLOETENS[19], Andrew M. DAVIS[21], Ryan DOLL[22], Christine FLOSS[22], George FLYNN[23], David FRANK[11], Zack GAINSFORTH[3], Philipp R. HECK[24], Peter HOPPE[25], Bruce HUDSON[26], Joachim HUTH[25], Brit HVIDE[9], Anton KEARSLEY[27], Ashley J. KING[28], Barry LAI[29], Jan LEITNER[25], Laurence LEMELLE[30], Hugues LEROUX[31], Ariel LEONARD[22], Robert LETTIERI[3], William MARCHANT[3], Larry R. NITTLER[32], Ryan OGLIORE[33], Wei Ja ONG[22], Mark C. PRICE[18], S. A. SANDFORD[34], Juan-Angel Sans TRESSERAS[19], Sylvia SCHMITZ[35], Tom SCHOONJANS[36], Geert SILVERSMIT[36], Alexandre SIMIONOVICI[37], Vicente A. SOLÉ[19], Thomas STEPHAN[21], Julien STODOLNA[3], Rhonda M. STROUD[38], Steven SUTTON[29], Mario TRIELOFF[6], Peter TSOU[39], Akira TSUCHIYAMA[40], Tolek TYLISZCZAK[13], Bart VEKEMANS[36], Laszlo VINCZE[36], Joshua Von KORFF[3], Naomi WORDSWORTH[41], Daniel ZEVIN[3], Michael E. ZOLENSKY[8], and > 30,000 Stardust@home dusters[42]

[1]Institut für Raumfahrtsysteme, University Stuttgart, Pfaffenwaldring 29, Stuttgart 70569, Germany
[2]Institut für Geophysik und Extraterrestrische Physik, Technische Universität Braunschweig, Braunschweig, Germany
[3]Space Sciences Laboratory, University of California Berkeley, Berkeley, California, USA
[4]European Space Agency, Madrid, Spain
[5]Max-Planck-Institut für Kernphysik, Heidelberg, Germany
[6]Institut für Geowissenschaften, Universität Heidelberg, Heidelberg, Germany
[7]Institut für Raumfahrtsysteme, University Stuttgart, Stuttgart, Germany
[8]Astromaterials Research and Exploration Science, NASA Johnson Space Center, Houston, Texas, USA
[9]Robert A. Pritzker Center for Meteoritics and Polar Studies, The Field Museum of Natural History, Chicago, Illinois, USA
[10]Deutsches Elektronen-Synchrotron, Hamburg, Germany
[11]Engineering and Science Contract Group, NASA Johnson Space Center, Houston, Texas, USA
[12]Naval Research Laboratory, Washington, District of Columbia, USA
[13]Advanced Light Source, Lawrence Berkeley Laboratory, Berkeley, California, USA
[14]Institut d'Astrophysique Spatiale, Orsay, France
[15]Geoscience Institute, Goethe University Frankfurt, Frankfurt, Germany
[16]Space Research Centre, University of Leicester, Leicester, UK
[17]Department of Astronomy, University of Washington, Seattle, Washington, USA
[18]School of Physical Sciences, University of Kent, Canterbury, Kent, UK
[19]European Synchrotron Radiation Facility, Grenoble, France
[20]Department of Earth and Planetary Sciences, University of New Mexico, Albuquerque, New Mexico, USA
[21]Department of the Geophysical Sciences, University of Chicago, Chicago, Illinois, USA
[22]Department of Physics, Washington University, St. Louis, Missouri, USA
[23]SUNY Plattsburgh, Plattsburgh, New York, USA
[24]Field Museum of Natural History, Chicago, Illinois, USA
[25]Max-Planck-Institut für Chemie, Mainz, Germany
[26]Midland, Ontario, Canada
[27]Natural History Museum, London, UK

[28]The University of Chicago and Robert A. Pritzker Center for Meteoritics and Polar Studies, The Field Museum of Natural History, Chicago, Illinois, USA
[29]Advanced Photon Source, Argonne National Laboratory, Chicago, Illinois, USA
[30]Ecole Normale Superieure, Lyon, France
[31]Université des Sciences et Technologies de Lille, Lille, France
[32]Carnegie Institution of Washington, Washington, District of Columbia, USA
[33]Hawai'i Institute of Geophysics and Planetology, University of Hawai'i at Manoa, Honolulu, Hawai'i, USA
[34]NASA Ames Research Center, Moffett Field, California, USA
[35]Institut für Geowissenschaften, Universität Frankfurt am Main, Frankfurt am Main, Germany
[36]Department of Analytical Chemistry, University of Ghent, Ghent, Belgium
[37]Institut des Sciences de la Terre, Observatoire des Sciences de l'Univers de Grenoble, Grenoble, France
[38]Materials Science and Technology Division, Naval Research Laboratory, Washington, District of Columbia, USA
[39]Jet Propulsion Laboratory, Pasadena, California, USA
[40]Department of Earth and Space Science, Osaka Univerisity, Osaka, Japan
[41]South Buckinghamshire, UK
[42]Worldwide
[†]Current address: International Space Sciences Institute (ISSI), Hallerstrasse 6, CH-3012 Bern, Switzerland
[*]Corresponding author. E-mail: veerle.sterken@issibern.ch

(Received 21 December 2012; revision accepted 10 September 2013)

Abstract–On the basis of an interstellar dust model compatible with Ulysses and Galileo observations, we calculate and predict the trajectories of interstellar dust (ISD) in the solar system and the distribution of the impact speeds, directions, and flux of ISD particles on the Stardust Interstellar Dust Collector during the two collection periods of the mission. We find that the expected impact velocities are generally low (<10 km s^{-1}) for particles with the ratio of the solar radiation pressure force to the solar gravitational force $\beta > 1$, and that some of the particles will impact on the cometary side of the collector. If we assume astronomical silicates for particle material and a density of 2 g cm^{-3}, and use the Ulysses measurements and the ISD trajectory simulations, we conclude that the total number of (detectable) captured ISD particles may be on the order of 50. In companion papers in this volume, we report the discovery of three interstellar dust candidates in the Stardust aerogel tiles. The impact directions and speeds of these candidates are consistent with those calculated from our ISD propagation model, within the uncertainties of the model and of the observations.

INTRODUCTION

NASA's Stardust mission was launched in 1999 with the goals of returning material from the coma of comet 81P/Wild 2 and returning material from the interstellar dust (ISD) stream entering the inner solar system (Tsou et al. 2003). For this purpose, one side of a collector (Stardust Interstellar Dust Collector, or SIDC) was used that consisted of 132 tiles of aerogel with a surface area of 1039 cm^2. There were also 150 cm^2 of Al foils, giving a total collector size of 0.12 m^2 (Tsou et al. 2003). The cometary particles have been the subject of extensive analyses since the return of the mission in 2006 (Brownlee et al. 2006). A preliminary examination of the aerogel tiles on the interstellar side of the collector led to an identification of three candidate interstellar dust (ISD) particles (Westphal et al. 2014), and the examination of the aluminum foils resulted in four possible ISD impact craters (Stroud et al. 2014). Calibration tests for the aerogel and foils were made at the Heidelberg Dust Accelerator and are described in Postberg et al. (2014), whereas Frank et al. (2013) discuss the statistical likelihood of the ISD candidates to be of an alternative origin.

Local ISD particles were detected for the first time in 1993 with the dust detector on Ulysses (Grün et al. 1993) and later also in the data of Galileo, Cassini, and Helios. Their properties, such as the derived upstream direction, were used to guide the planning for the Stardust mission. Predictions of the statistics of ISD to be captured by Stardust were first made by Landgraf et al. (1999b), using a model consistent with the Ulysses and Galileo observations of interstellar dust. Two ISD populations were assumed: one with radiation pressure constant $\beta = 1$ ("small particles") and one with $\beta = 0.1$ and charge-to-mass ratio Q/m = approximately 0 C kg^{-1} ("large particles"). (Here, β is the dimensionless ratio of

the force due to solar radiation to solar gravitational force). Small particles are strongly affected by electromagnetic forces, and the flux assumed for these particles was one-third of the original flux measured by Ulysses and Galileo. The "large" particles were estimated to be about 10% of the total Ulysses and Galileo flux (based on the data), but their flux is not reduced by electromagnetic forces. The total duration of the collection period was assumed to be 290 days. Eighty small and 40 large particles were predicted to be captured in total. The large particles were predicted to have an impact velocity between 20 and 40 km s^{-1} for the collection periods assumed in the study, based on the collection period of 290 days. These predictions were a good first estimate, but the total duration of exposure actually experienced by the SIDC was shorter than assumed in the preflight modeling of Landgraf et al. (1999b). Therefore, we provide an updated prediction of the number of particles captured by Stardust under the model, using updated information of the collection periods, a larger parameter space of particle properties and using the Ulysses measurements in combination with dust trajectory simulations as a starting point for the absolute number predictions. In contrast to Landgraf et al. (1999b), we also assume a continuum of β-values rather than only two different populations (small/large).

SIMULATING INTERSTELLAR DUST TRAJECTORIES

On the basis of a model compatible with the Ulysses and Galileo observations, we calculate interstellar dust flux and velocities (trajectory and speed) through the heliosphere. In this section, we describe the assumptions adopted for the simulations and the interstellar dust dynamics in the heliosphere, which causes a "filtering" of the particles in the inner solar system.

Initial Interstellar Dust Direction and Speed

The Sun and the heliosphere move through a dense warm cloud of dust and gas (mainly H and He), called the local interstellar cloud (LIC). Because of this relative movement, the interstellar neutral gas sweeps through the heliosphere at an average speed of about 26 km s^{-1} (Witte et al. 1993) with respect to the Sun and comes from one apparent mean direction[1]: 259° longitude and +8° latitude in the ecliptic frame (Landgraf 1998; Frisch et al. 1999). A thorough discussion on the relative motion of the solar system with respect to the LIC and other neighboring clouds is given in Linsky et al. (2008). McComas et al. (2012) reported that the heliosphere is moving slower with respect to the ISM than previously thought (23 km s^{-1} instead of 26 km s^{-1}) and that, therefore, no bow shock forms upstream of the heliosphere. During this study, we assumed the nominal initial flow direction to be 259° ecliptic longitude and +8° ecliptic latitude and the initial speed of the interstellar particles is assumed to be 26 km s^{-1}; this assumes that the interstellar gas and dust are closely coupled, and is consistent with Ulysses in situ data of interstellar dust (Witte et al. 1993). Although we assume these values for the calculations, the real velocity and direction may be more dispersed due to the influence of heliopause, heliosheath, and termination shock. Taking these effects into account is beyond the scope of this study. Slavin et al. (2012) calculated such trajectories including the effects at the heliopause and termination shock, but the time-varying interplanetary magnetic field was not yet taken into account for the relevant flight time of the particles.

[1]The 1σ and 2σ values are for the longitude ($+2\sigma$) 290°, ($+1\sigma$) 275°, (-1σ) 245°, (-2σ) 210° and for the latitude ($+2\sigma$) 15°, ($+1\sigma$) 12°, (-1σ) 5°, (-2σ) 0° (Landgraf 1998; Frisch et al. 1999).

Interstellar Dust Dynamics

Interstellar dust trajectories in the solar system are dominated by solar gravity, solar radiation pressure force, and Lorentz forces resulting from the interaction of the charged dust particles with the interplanetary magnetic field (IMF). How these three forces modify the ISD flow in the solar system, depending on the particle parameters β and Q/m, is described in detail in Sterken et al. (2012a). Its influence on the ISD size distribution in the solar system is described in Sterken et al. (2012a).

As both the solar gravity and solar radiation pressure forces decrease quadratically with increasing distance from the Sun, we combine both forces in one expression. The ratio of the solar radiation pressure force to the force of solar gravity ($\beta = F_{RP}/F_G$) determines whether the ISD particles are repelled from or attracted to the Sun. The value of β depends mainly on particle size, the optical properties of the particle surface material, and the particle surface morphology. Particles with $\beta < 1$ move in hyperbolic orbits around the Sun and a focusing of these particles exists "downstream" from the Sun. Particles with $\beta = 1$ move on straight trajectories through the solar system. Particles with $\beta > 1$ are repelled from the Sun and therefore are not able to penetrate a paraboloidal-shaped region around the Sun. This region is called the *β-cone* and is larger and farther away from the Sun for particles with higher β-value.

Lorentz forces also influence the trajectories of the ISD particles. As the interstellar dust particles move through the solar wind plasma, they collect ions and electrons from this plasma, lose electrons by secondary electron emission and by photoionization in sunlight. The latter is the dominant effect and the ISD particles typically become charged to a potential of about +5 V for particles in the inner heliosphere larger than 0.2 μm[2]. The smaller the particle, the larger the charge-to-mass ratio Q/m, and the larger the Lorentz forces that arise when a charged particle moves through the ambient solar wind magnetic field. The interplanetary magnetic field is dragged out from the Sun by the solar wind and is described by the Parker spiral. The magnetic field in the solar wind changes with the solar cycle: during the solar minimum, the solar magnetic field has a dipole-like structure, which becomes mixed at solar maximum, but comes back to a dipolar field with opposite polarity in the next solar minimum. When the polarity of the IMF is positive in the northern heliosphere and negative in the southern, a particle passing through this magnetic field will experience a Lorentz force that bends it away from the solar equatorial plane (which is almost aligned with the ecliptic plane). At the next solar minimum when the direction of the IMF is reversed, the particles will be focused toward the solar equatorial plane. Hence, every 22 years, there will be an 11-year defocusing phase of the solar cycle with respect to the interstellar dust particles, and followed by an 11-year focusing phase (Landgraf et al. 2000; Sterken et al. 2012a). The phase of the solar cycle during the period in which the Stardust mission was exposed to the interstellar dust stream was the last part of the defocusing phase.

Filtering at the Termination Shock

Besides the filtering in the inner solar system, the ISD particles are also filtered at the edge of the heliosphere between the heliopause and the termination shock. Compared with conditions in the undisturbed interstellar space, particles become more charged because of the denser, higher temperature plasma (more secondary electron emission) and also the magnetic field is stronger at the heliosphere boundary. Therefore, the Lorentz force is locally enhanced. The filtering at the termination shock has been calculated by Linde and Gombosi (2000) and Slavin et al. (2010). These authors found that generally only particles with radius bigger than 0.1 μm are able to pass through the heliospheric boundary (for a defocusing configuration of the IMF). Smaller particles have thus been filtered out at the termination shock. Slavin et al. (2012) calculated the densities of ISD in the outer and inner heliosphere for the focusing and defocusing configuration of the IMF. They found that small particles can also be focused and thus pass the boundary regions of the heliosphere, but they did not take the time variation in the IMF into account during the particles' flight time. This filtration (or focusing) by the termination shock was not taken into account in the simulations in this study, as the flux estimate is based on the Ulysses data in the inner solar system and not on the original ISD size distribution in the LIC.

[2]Particle potentials of 2–7 V were reported by Kempf et al. (2004). These were measured for interplanetary dust. Slavin et al. (2012) calculated ISD potentials between about 5 and 9 V for particles between 0.1 and 1 μm.

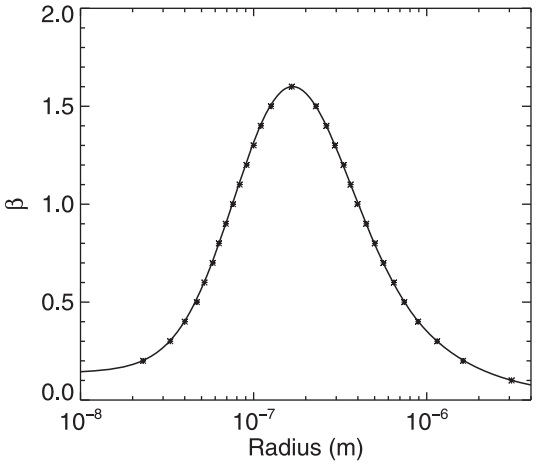

Fig. 1. The assumed reference β-curve, adapted from Gustafson (1994) and with a maximum of $\beta_{max} = 1.6$ to be consistent with the results of Landgraf et al. (1999a). This curve relates β-values to particle radii for one certain material. The β-values used for the calculations of Figs. 8, 9, 10, 12, and 14 are indicated in the curve with stars.

Material Assumptions: The β-curve

The relationship between β-value and particle radius for a certain material is called the "β-curve" and has been derived experimentally by Gustafson (1994) and theoretically by Kimura et al. (2002) and Schwehm (1976). The β-curve used in the calculations here is that for astronomical silicates as given by Gustafson (1994), but adapted to the outcome of the Ulysses data analysis of Landgraf et al. (1999a). These authors concluded from the measured ISD mass distribution in the Ulysses data between 1992 and 1999 that the decrease in observed flux for particles with mass between 1×10^{-17} and 3×10^{-16} kg is due to particles that have β-values of 1.6. Therefore, the maximum β-value in the β-curve we use (the "reference β-curve") in our model is 1.6. The density assumed for this hypothetical β-curve is 2 g cm^{-3}. Our reference β-curve is shown in Fig. 1. The average β-value of ISD particles is $\beta = 1.1$ (Landgraf

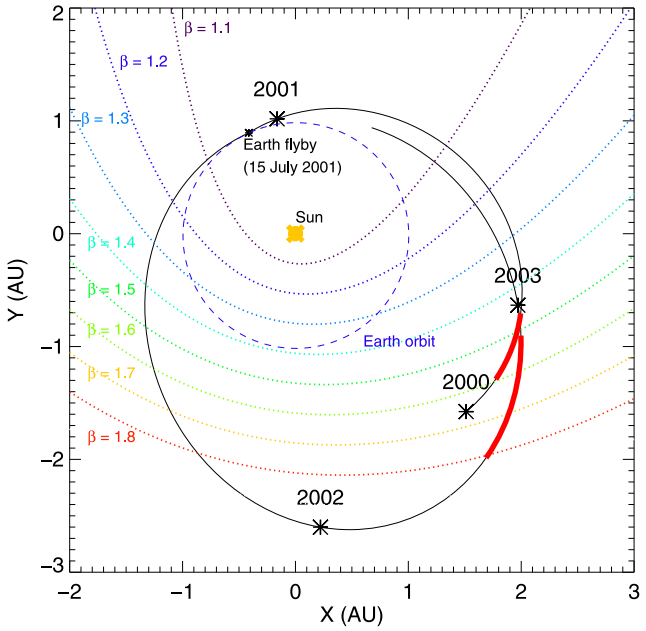

Fig. 2. The orbit of Stardust with respect to the β-cones. The red thick lines are the two ISD capture periods.

et al. 2003), corresponding to a typical radius of about 0.3 μm. For a given β-value, two particle sizes are possible: a small one or a large one. However, the small particle branch is strongly reduced by the filtering at the heliopause and plays no major role in the analysis of the Stardust particles.

The Stardust Collection Periods and Attitude

The orbit of Stardust with respect to the β-cones is shown in Fig. 2. The red thick lines in the plot correspond to the collection periods (February 22, 2000 until May 1, 2000 and August 5, 2002 until December 9, 2002 [Tsou et al. 2003], 195 days in total).

Both collection periods are partially inside the $\beta = 1.8$ cone, i.e., not allowing particles with $\beta > 1.8$ to be captured. During about half of the collection time, particles with β between 1.5 and 1.6 are missing, especially toward the middle and the end of the first collection period, and toward the end of the second collection period. Under our model, Stardust would not capture particles of radius roughly between 0.12 and 0.25 μm during these parts of the collection period.

During the collection periods, the Stardust collector was pointed into the nominal interstellar dust stream for which it was assumed that the particles have $\beta = 1$ and are coming from an ecliptic longitude of 259° and ecliptic latitude of +7.7° (JPL, N. 2012, Stardust SPICE kernels, http://naif.jpl.nasa.gov/naif/). The relative speed of the ISD particles with respect to the spacecraft was taken into account for the pointing direction of the collector. However, the real pointing of the collector varies from this nominal direction. Figure 3 shows the ideal pointing direction of the cometary side of the collector in the heliocentric ecliptic frame as a smooth curve and the real (commanded) pointing as a wiggly curve around the ideal pointing direction. Such excursions in pointing as shown in Fig. 3 lead to an uncertainty of about 15° in the impact direction derived from the tracks ($1\sigma = \pm 24.8°$ and $\pm 7.7°$ for the longitude and latitude and with a mean of $-6°$ and 0.65°, respectively, for the two periods together). A histogram of the pointing deviation from the nominal direction is shown in Fig. 4 for the two collection periods together. The percentage of time in which Stardust points within a certain angle from the nominal pointing direction is shown in Fig. 5: about 80% of the

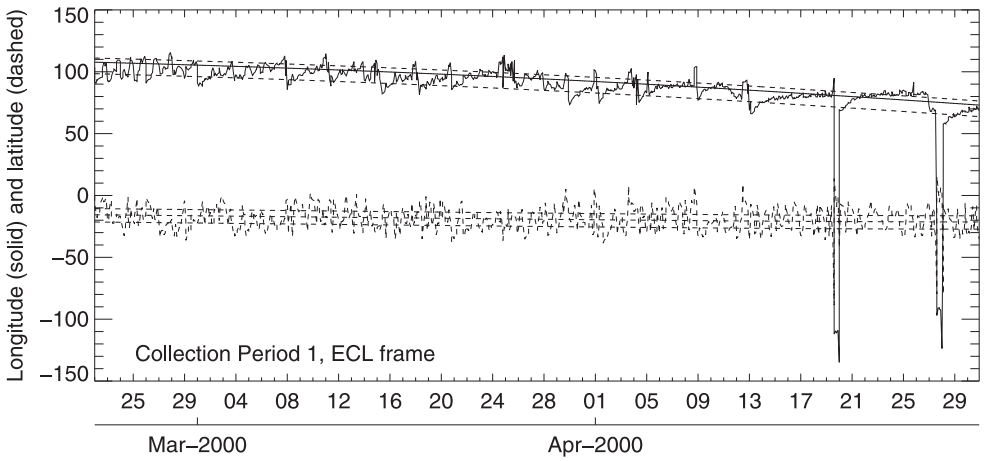

Fig. 3. The ideal pointing and commanded pointing of the Stardust IDC in the first collection period. The solid line shows the longitude and the dashed line shows the latitude in the heliocentric ecliptic frame. The two dashed lines above and below each are the calculated dispersion ($1\sigma = \pm 24.8°$ and $\pm 7.7°$ for the longitude and latitude with a mean of $-6°$ and 0.65°, respectively, for the two periods together).

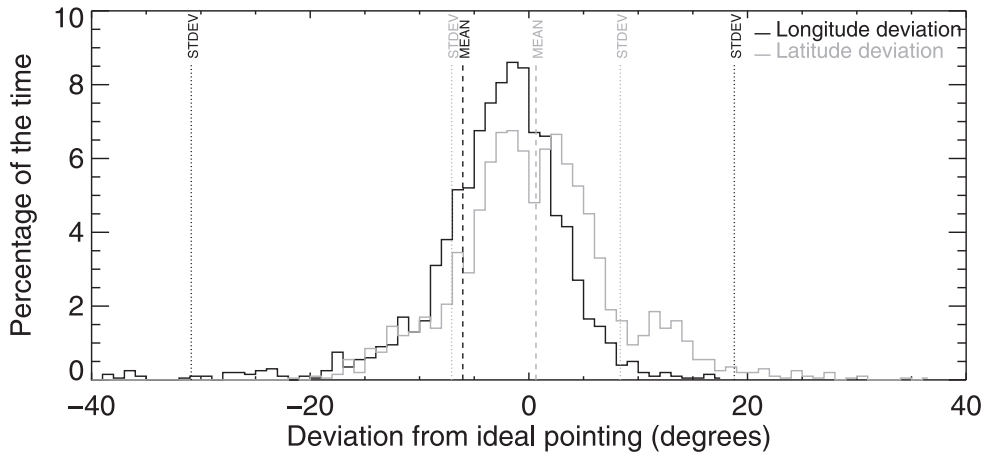

Fig. 4. A histogram of the pointing deviation from the nominal pointing direction, for the longitude (black line) and the latitude (gray line). Values below −40° are not shown. The averages and standard deviations are also indicated ($1\sigma = \pm 24.8°$ and $\pm 7.7°$ for the longitude and latitude with a mean of −6° and 0.65°, respectively, for the two periods together).

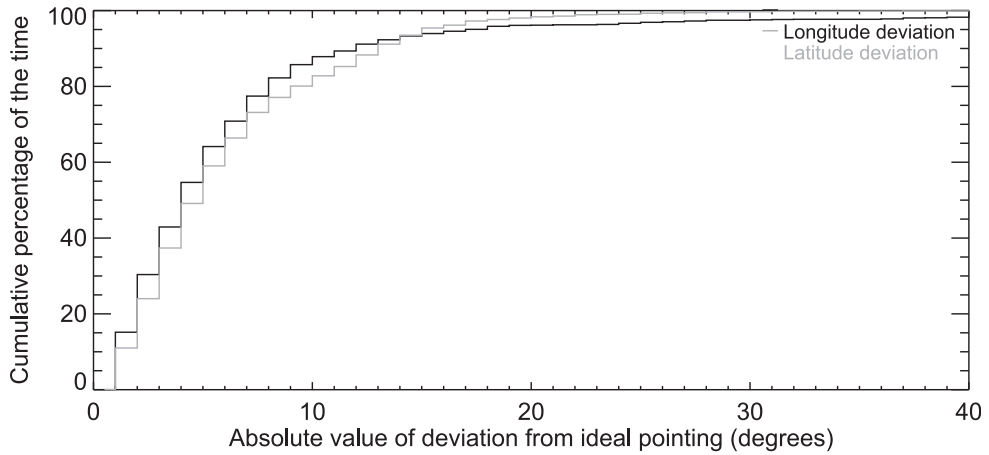

Fig. 5. The cumulative percentage of time that Stardust points within a certain angle from the nominal pointing direction, for the longitude (black line) and latitude (gray line). Both are about 80% of the time within 10° of the nominal pointing direction.

time, the longitude and the latitude are within 10° from the nominal pointing direction.

RESULTS

Influence of the Lorentz Force on the Flux

The collection period occurred a few years after the solar minimum of the "defocusing cycle." Therefore, the particles were defocused from the solar equatorial plane by Lorentz forces and thus most ISD particles on the "smaller" side of the β-curve (i.e., ~ <0.15 μm) will probably not have made it to the inner solar system or at least their flux will be strongly reduced. Also, the flux of such small particles may be strongly reduced or filtered (or locally enhanced, cf. Slavin et al. 2012) at the termination shock (Linde and Gombosi 2000; Slavin et al. 2010).

The relative flux in the inner heliosphere with respect to the incoming flux after passing the termination shock was calculated for the period between 2000 and 2003 at both the Ulysses and Stardust positions. This was done for seven different particle masses corresponding to a charge-to-mass ratio Q/m of 0.125, 0.5, 1, 1.5, 3, 6, and 12 C kg^{-1} (Sterken et al. 2012a) and having a β along the assumed β-curve. How these Q/m-values relate to particle radius is illustrated in Table 1 for particles with density of 2 g cm^{-3}. Smaller particle densities will enhance the electromagnetic interaction. Figure 6 shows on the left the relative flux in the inner solar system with respect to the incoming flux for both Ulysses (between 2000 and 2003) and Stardust (2000 and 2002). In Fig. 6, particles with mass $<3 \times 10^{-17}$ kg (corresponding to a charge-to-mass ratio $Q/m > 3$ C kg^{-1} [Sterken et al. 2012a] and collection period in 2000), and 6 C kg^{-1} (1×10^{-17} kg, collection period 2002), respectively, are totally filtered out or strongly reduced to less than 10% of the original flux. Note that the largest particles are not enhanced due to

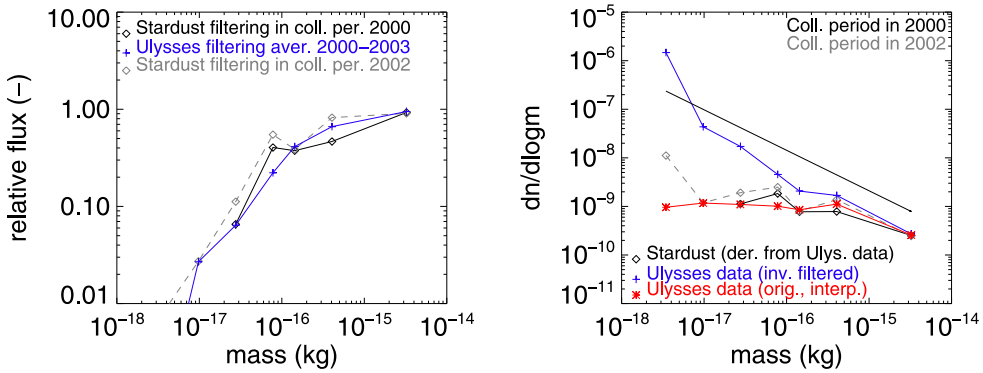

Fig. 6. Left: The relative flux of ISD particles with mass due to the filtering in the inner heliosphere is shown for the Ulysses mission and the two collection periods of the Stardust mission. Right: Number density of particles for Ulysses (red stars) between 2000 and 2003 (Krueger, personal communication), the "original size distribution" at 50 AU upstream from the Sun, derived from the Ulysses data (blue crosses) using the model, and the final derived number distribution for Stardust (black diamonds). The straight black line is an extrapolation of the Mathis et al. (1977) size distribution to the range of simulated masses. The reference β-curve is used and the particle density ρ is assumed to be 2 g cm^{-3}. For the MRN-distribution, a hydrogen number density of n_H = 0.3 cm^{-3} is used.

Table 1. Overview of particle masses, β-values, Q/m, and corresponding particle radii assuming a density ρ = 2 g cm^{-3}, particle potential U = +5 V, and the reference β-curve.

Mass (kg)	β	Q/m (C kg^{-1})	Radius (μm)
3.2×10^{-15}	0.5	0.125	0.73
4.1×10^{-16}	1.1	0.5	0.36
1.4×10^{-16}	1.4	1.0	0.26
7.8×10^{-17}	1.5	1.5	0.21
2.8×10^{-17}	1.6	3.0	0.15
9.6×10^{-18}	1.4	6.0	0.11
3.5×10^{-18}	1.0	12	0.07

gravitational focusing because neither Ulysses nor Stardust is positioned downstream from the Sun. These particles have a relative flux of 1 because they are not filtered by solar radiation pressure force (very low β) nor enhanced by gravitational focusing.

The red line in Fig. 6 (right) shows the Ulysses measured number distribution per log(m), from Krüger (personal communication) between 2000 and the beginning of 2003 and interpolated to the seven masses corresponding to the Q/m-values mentioned above. From these observations, the ISD number distribution at the heliospheric boundary (inside the termination shock) is calculated using the model in the opposite direction (blue line in Fig. 6, right-hand side): instead of multiplying the original size distribution with the reduction factor from the simulations, we divide the measurements of Ulysses by this factor to get an "unfiltered" original distribution, 50 AU upstream from the Sun. The final filtered ISD number distribution for the Stardust mission is shown by the black line in this figure. The expected number distribution for Stardust is thus made consistent with the Ulysses measurements, taking into account the different positions of the two spacecraft. For a comparison to these measurements and derivations, an extrapolation of a general ISD size distribution as modeled by Mathis et al. (1977) (the so-called "MRN-distribution") to the particle radii of the simulations is shown as a straight line for a hydrogen number density n_H = 0.3 cm^{-3} and dust particle density of 2 g cm^{-3}. This distribution was not used for the Stardust flux calculations as these are based on the Ulysses measurements.

Influence of the Lorentz Force on the ISD Velocity and Direction

Simulations were also made for different combinations of β and Q/m (cf. Sterken et al. [2012a, 2012b] in total 70 combinations) to study the sensitivity of the relative flux, impact velocity, and ISD flow direction on the selected particle parameters. The outcome was as follows:

1. The relative flux decreases strongly with increasing Q/m (thus with decreasing mass) as is also indicated in Fig. 6. Moreover, the flux also becomes zero for particles with β-value larger than the β-cone where Stardust is located. Therefore, the estimate of the flux of particles on Stardust is made using a simulation program that includes Lorentz forces, however, at the cost of model precision. The full simulation uses a grid size of 1.5 AU around the Sun (Sterken et al. 2012a), and "only" seven masses are simulated for computation time reasons.
2. The impact speeds vary only little with increasing Q/m within the collection time and position of Stardust: for the same β-value but different Q/m,

Table 2. Overview of expected amount of particles impacting on the Stardust collector (both front- and backside) for masses larger than the mass indicated. These numbers are derived from Ulysses measurements using the ISD model from Sterken et al. (2012a) that includes Lorentz forces. The estimates assume the reference β-curve and an average impact velocity of 10 km s^{-1}. The radii of the particles corresponding to the given masses are indicated for three assumed particle densities (2, 1, and 0.5 g cm^{-3}).

Mass (kg)	Radius (μm) ρ = 2 g cm^{-3}	Radius (μm) ρ = 1 g cm^{-3}	Radius (μm) ρ = 0.5 g cm^{-3}	Period 1	Period 2	Total
3.2×10^{-15}	0.73	0.91	1.15	0.4	0.7	1.1
4.1×10^{-16}	0.36	0.46	0.58	2.9	8.8	11.7
1.4×10^{-16}	0.26	0.32	0.41	5.2	13.1	18.3
7.8×10^{-17}	0.21	0.27	0.33	10.7	26.6	37.3
2.8×10^{-17}	0.15	0.19	0.24	14.1	37.5	51.6
9.6×10^{-18}	0.11	0.13	0.17	14.1	44.1	58.2
3.5×10^{-18}	0.07	0.09	0.12	14.1	109.7	123.8

the velocity difference is maximum 4 km s^{-1} (within the collection periods). Therefore, for further investigation of the impact speeds, we neglect the Lorentz force and use simulations with solar radiation pressure force and gravity only, for the benefit of having a precision of 0.1 AU from Stardust instead.

3. The absolute ISD latitude at Stardust varies only slightly (maximum 10°) and depends more on Q/m than on β, whereas the longitude varies more (up to 30°) and depends mostly on the β-value of the particles. The absolute longitude of the (downstream pointing) ISD velocity vector decreases as the β-value of the particle approaches the β-value of the β-cone where Stardust is located. This is as expected since the closer to the β-cone, the more the particle trajectory will deviate from its original path due to the solar radiation pressure force. Because the direction does not change dramatically with Q/m, we investigate further the directions of the particles using only solar radiation pressure force and gravity, but with a precision of 0.1 AU from Stardust.
4. The strong dependence of the ISD impact speed and direction on β and the small influence of Q/m during these two collection periods and at Stardust location are only valid for β-values smaller than the β-cone where Stardust is located (see Fig. 2). For β-values close to the β-cone at Stardust location, the impact directions can vary much more depending on Q/m. For those particles ($\beta \approx \beta$-cone value at Stardust and thus $V \approx V_{rel}$), due to a small change in Q/m, the relative longitudes could theoretically take on any value.

Estimating the Absolute Number of Impacts on Stardust

We estimate the absolute number of impacted ISD particles on Stardust, using the Ulysses data and the simulations. This excludes any secondary population arising from impacts on the collector by ejecta from primary impacts elsewhere on the spacecraft surface (see Burchell et al. [2012] for a discussion). The calculation for the predicted number density is based on the measured number density from Ulysses (Krueger, personal communication) and takes into account the effective instrument surface of Stardust and Ulysses, as well as their observation times and the simulation results at Stardust and Ulysses location and time. We also assume an average impact velocity of 10 km s^{-1} for the calculation of the fluxes from densities. The average impact speed depends strongly on the assumed beta curve and particle size distribution, so these results can be scaled using the average impact speed of any chosen interstellar dust model. The total estimated number of detectable particles in the aerogel is about 50 (cf. Table 2; Fig. 7), based on a minimum detectable particle radius of about 0.15 μm (Postberg et al. 2014). So far, only three candidates of interstellar particles have been identified.

ISD Impact Speeds on Stardust

We study the variation in the impact speeds with the particle radius for six different times during the collection periods, namely at the beginning, middle, and end of each period. The collection speeds of ISD particles are calculated from the trajectory simulations where only solar radiation pressure force and gravity are taken into account. Figure 8 shows the dependence of the simulated impact speeds of the particles on β, at the six times indicated. As explained by Sterken et al. (2012a), the ISD velocity at a fixed location decreases with increasing β-value. Note that the *relative* velocity for the ISD particles increases again for the biggest β-values. This is because the particles with the largest beta are moving more slowly relative to the Sun than Stardust in its orbit; thus, Stardust may overtake the

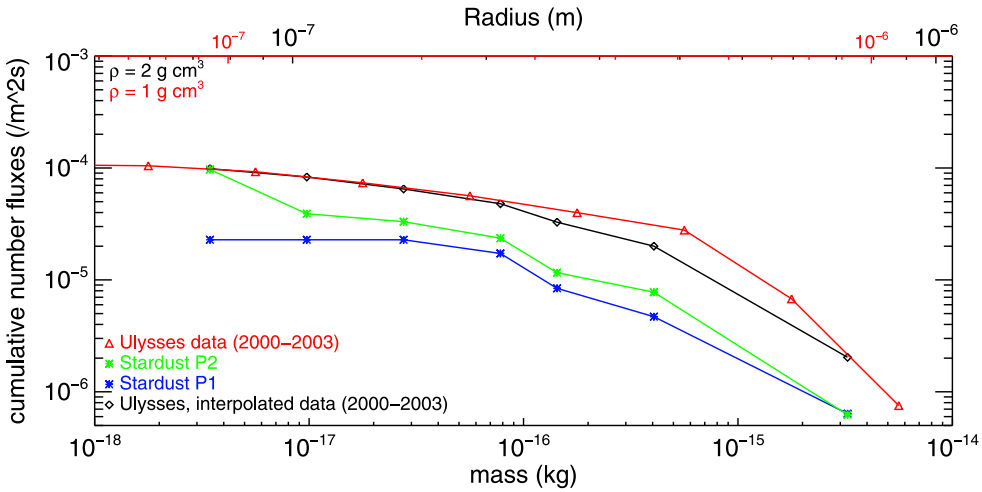

Fig. 7. The simulated cumulative flux of ISD particles with mass for the two periods of the Stardust interstellar dust collection. The original Ulysses data between 2000 and 2003 (Krueger, personal communication) are shown as a red line; the interpolation of the data to the seven simulation points is shown as a black line; and the green and blue lines show the simulated cumulative ISD flux for the two collection periods of the Stardust mission. The reference β-curve is used and the particle density ρ is assumed to be 2 and 1 g cm^{-3}, respectively (top axis).

ISD particles that, as a consequence, may impact on the cometary side of the collector. This has been found for some epochs by calculations of the impact directions. In the last part of the two collection periods, particles with $\beta > 1.5$ and 1.6, respectively, will be missing because Stardust is inside the β-cones for these values. Note that the *relative* velocity of the particles depends on the *absolute* ISD velocity as well as on the spacecraft velocity vector, which is different at different epochs of the collection period. Therefore, particles with equal β-value (e.g., $\beta = 1$) have different impact speeds at different times.

When we assume the reference β-curve, we find a relation between impact speed and particle radius, as shown in Fig. 9. The left-hand side of the plot is hatched for particles smaller than 0.15 μm to indicate the filtering at the heliosphere boundary.

Based on these assumptions, ISD particles between 0.25 μm and 0.4 μm radii have impact speeds between 3 and 14 km s^{-1}, depending on when, during the collection period, they are captured. Particles between 0.4 and 0.7 μm have impact speeds between 10 and 20 km s^{-1} and particles larger than 0.7 μm have impact speeds of 14–25 km s^{-1}. The gaps in the speed curves (Fig. 9) around particle radius 0.16 μm (from roughly 0.12–0.23 μm) are consequences of the β-cone for $\beta = 1.5$.

Impact Direction

The ISD impact directions on the Stardust collector also change depending on β and thus on particle size. The largest shift in directionality occurs for particles with β close to maximum β-value that can reach Stardust, i.e., around $\beta = 1.5$ to $\beta = 1.6$. The absolute ISD latitudes change by only a few degrees, whereas the absolute longitudes change by up to 30° for particles of about 0.25 μm. This has a large influence on the zenith and azimuth angle of the ISD impact direction on the collector. In the simulations discussed in this section, we do not consider the effects of the spacecraft pointing variations, which adds to the uncertainty, but we assume a perfect pointing in the *relative* ISD particle velocity direction for particles with $\beta = 1$ and a radiant at 259° ecliptic longitude and +8° ecliptic latitude (Landgraf et al. 2000).

The zenith angle of the ISD impact direction on the collector is defined as the angle of the relative ISD velocity vector to the collector normal on the cometary side. The zenith angle is thus zero for particles impacting along the collector normal and >90° for particles impacting on the cometary side of the collector. The azimuth angle is the angle of the relative ISD velocity vector, projected on the collector surface. It is 0° away from the spacecraft body (thus in the direction pointing toward the Sun) and 180° in the direction of the spacecraft body. (A schematic drawing is shown in Fig. 11.)

Stardust Measurements

The impact directions of the three preliminary ISD particle candidates have been determined from the tracks in the collector (Westphal et al. 2014). Their zenith angles were 28°, 41°, and 51°. They all have azimuth angles within 20° from the Sun direction (0° azimuth). A zenith angle uncertainty due to the

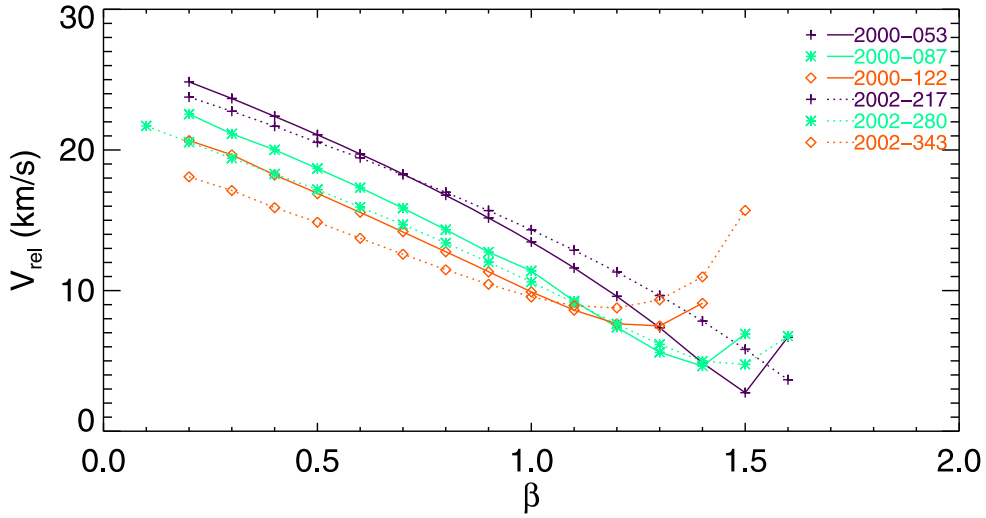

Fig. 8. The simulated impact speeds with β-values of the particles at six times during the two collection phases of the Stardust mission. Lorentz forces are not taken into account in this plot. The dates for which these speeds are calculated are labeled as "year – day-of-year."

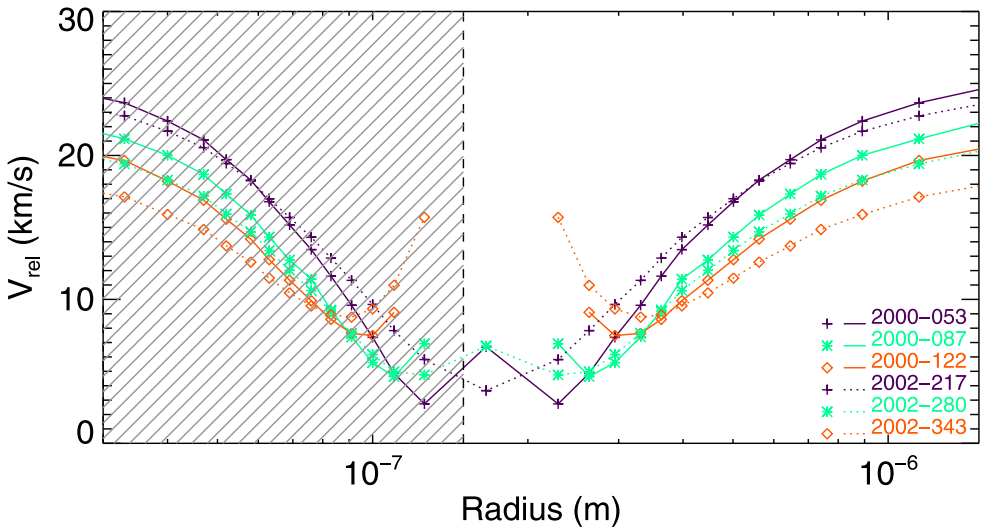

Fig. 9. The calculated impact speeds for different particle radii (in meter) and for six different times during the collection phase of the Stardust mission, labeled as "year – day-of-year." The reference β-curve was assumed and a particle density of 2 g cm^{-3}. Lorentz forces were not taken into account. Therefore, the hatched region denotes the radii of particles of which large or total filtering is expected (see also Fig. 6 and Table 2). The larger particles will be fast, but may be less abundant in absolute number. Very small particles are filtered out by Lorentz forces.

spacecraft pointing is estimated to be ±15°. This is the dominant source of uncertainty in impact direction reconstructed from the track in the aerogel as it has been shown (Burchell et al. 1998, 2012) that aerogel tracks indicate the preimpact trajectory to within better than 1–2°. The (average) 15° wiggle in the spacecraft pointing does not translate in a similar excursion in zenith angle. A better error analysis could be done, but is beyond the scope of this study. The impact speed of the particles was estimated from the track sizes and shapes (Postberg et al. 2014; Westphal et al. 2014): particles of tracks 30 and 34 have probable impact speeds below 10 km s^{-1} and the particle of track 40 had an impact velocity above 15 km s^{-1}.

Figure 10 shows the simulated impact zenith angles on the collector for an initial dust direction of 259°, assuming a perfect spacecraft pointing in the relative ISD direction of the ISD flow. In the beginning of the second collection period (2002-d217), Stardust is still far away from the β = 1.6 cone and the zenith angle on the

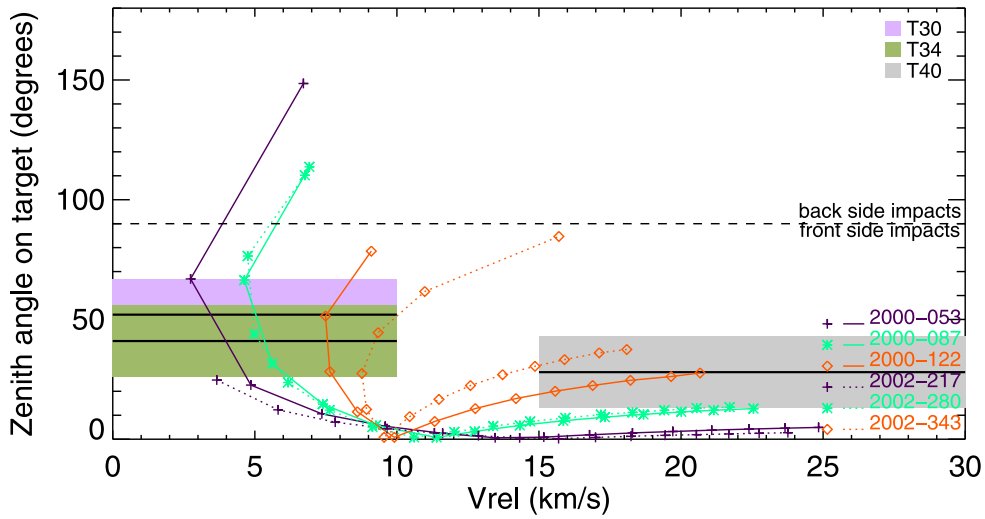

Fig. 10. The zenith angle of the ISD impact direction on the Stardust collector with increasing impact speed is shown for six epochs during the two collection periods, which are labeled as "year – day-of-year." A zenith angle larger than 90° indicates that the particles are impacting on the cometary side of the collector. The zenith angles of the three ISD candidates found in the aerogel (Westphal et al. 2014) and a 15° pointing uncertainty are indicated (colored regions). The color labels T30, T34, and T40 correspond to track 30, 34, and 40 (Westphal et al. 2014).

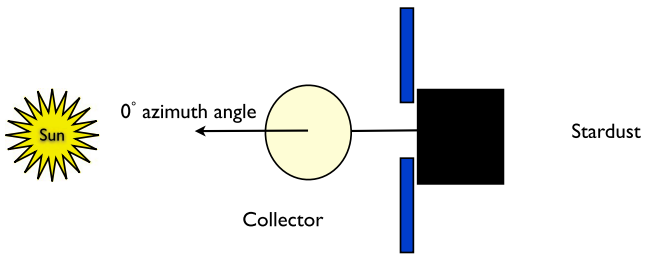

Fig. 11. Schematic drawing of the definition of the azimuth angle.

collector will remain close to the collector normal. For higher β-values and later times in the collection periods, the zenith angle deviation increases as Stardust is closer to the cones. Particles with $\beta = 1$ move on straight trajectories through the solar system at all times, so if assuming an "ideal" spacecraft pointing, these particles have about 0° impact zenith angles on the collector (see Fig. 10). Particles with zenith angle larger than 90° will impact on the cometary side of the collector. This is not only because the (absolute) longitude of the ISD changes when Stardust is closer to the β-cones but also because the absolute velocity of the particles with β close to 1.5 and 1.6 gets lower and approaches the spacecraft velocity. Hence, Stardust "overtakes" some of the interstellar dust particles, which then impact on the cometary side of the collector.

The range of impact speeds and zenith angles that were found from track size, shape, and direction are also shown in Fig. 10 and they overlap the speeds and zenith angles from the simulations very well.

Figure 12 shows the simulated azimuth angles on the Stardust collector with impact speed. Also in Fig. 11, we plot the azimuth angles from the three tracks, including an estimated 15° to illustrate the spacecraft pointing error. Here, only for track 40 is there much overlap between the velocities and azimuth angle from the track and the simulations. Again, this is independent of the particle density or β-curve assumed, but an initial ISD direction of 259° longitude and ideal spacecraft pointing are assumed. There seems to be an inconsistency with the expected impact azimuth angle for tracks 30 and 34. However, by modifying the assumptions about the ISD direction, well within their uncertainties, an agreement can be found. The particles with the highest speeds correspond to $\beta < 1$ particles and they impact in the direction toward the Sun (0° azimuth). The particles with $\beta = 1$ have undetermined azimuth angles as their impact velocity vector is close to the collector normal, i.e., they have a zenith angle of 0°. Also in Fig. 12, we plot the azimuth angles from the three tracks, including an estimated ±15° to illustrate the spacecraft pointing error. Here, only for track 40 is there much overlap between the velocities and azimuth angle from the track and the simulations. Again, this is independent of the particle density or β-curve assumed, but an initial ISD direction of 259° longitude and ideal spacecraft pointing are assumed.

Most interstellar dust impacts occur close to a plane through the collector normal in the 0–180° azimuth direction. We can project the impact direction onto that plane and define a "capture zenith angle," which is the zenith angle, multiplied by the cosine of the azimuthal

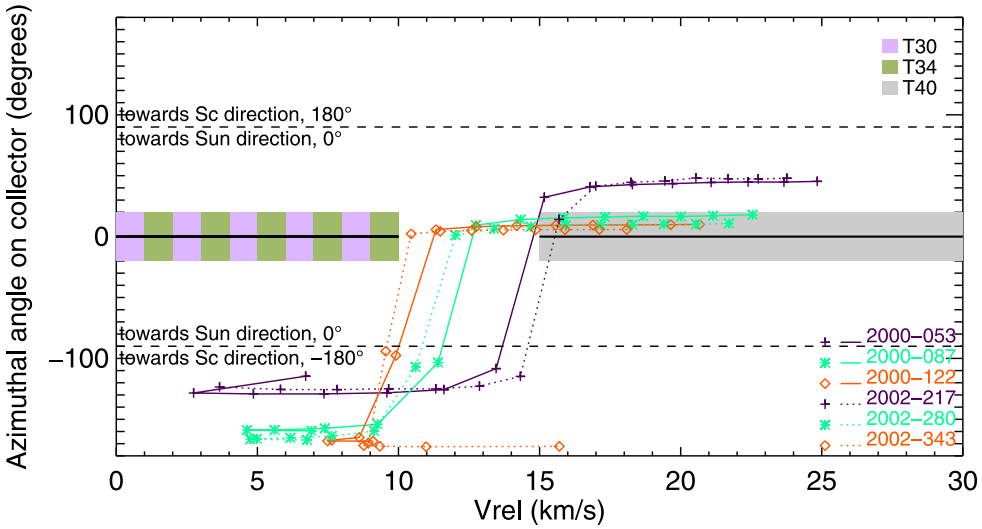

Fig. 12. The azimuth angle of the ISD impact direction on the Stardust collector with increasing impact speed is shown for six epochs during the two collection periods and inflow direction 259°. The azimuth angles of the three ISD candidates found in the aerogel (Westphal et al. 2014) and a 15° pointing uncertainty are indicated (colored regions). The color labels T30, T34, and T40 correspond to tracks 30, 34, and 40 (Westphal et al. 2014), respectively.

angle. Figure 13 shows this "capture zenith angle" for three different initial directions of the incoming dust with the relative speed. Values below zero indicate azimuthal angles in the spacecraft direction (180° azimuth), whereas positive values indicate azimuthal angles toward the Sun direction (0° azimuth). The zenith angles extracted from the tracks of the three preliminary ISD particles in the collector (Westphal et al. 2014) are indicated in the plot as horizontal lines surrounded by colored error boxes. A first brief look at the Stardust results with respect to the modeling reveals that for the average inflow direction of 259°, only one particle fits the simulations (track 40). If all three particles are of interstellar origin, then the 274° inflow direction fits better. However, because of the large statistical uncertainty (only three ISD impacts) and the uncertainties in the determination of the exact impact direction and uncertainties in the modeling assumptions, this result is not definitive. Regardless of model uncertainties, we find under this model that interstellar dust should cluster in azimuth around 0° (the so-called "midnight" direction, toward the Sun) and 180° (antisunward) (Westphal et al. 2014). In a companion paper (Frank et al. 2014), it is shown that the arrival directions of interplanetary dust particles peak around ±90°, with a strong depletion at 0° and 180° for off-normal (zenith angle $> \sim 20°$) tracks. Thus, because the distributions of azimuths of interstellar and interplanetary dust populations are distinct, and azimuth, at least in a statistical sense, can discriminate between different origins (Frank et al. 2013; Westphal et al. 2014) the distribution of the three candidates is most consistent with an interstellar origin; an interplanetary origin is statistically less likely.

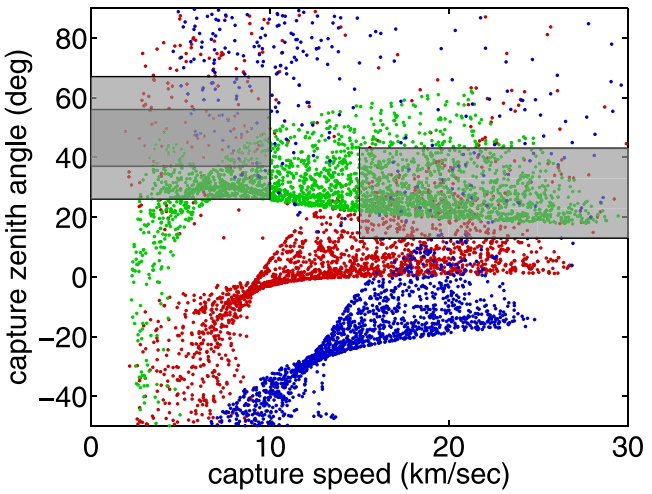

Fig. 13. The "capture zenith angle" (the zenith angle multiplied by the negative cosine of the azimuthal angle) for three different directions of the incoming dust: 244° (blue), 259° (red), and 274° (green) plotted against the impact velocity. The capture zenith angles of the three identified ISD candidates (Westphal et al. 2013) are indicated as gray boxes.

With an assumed β-curve and material density, we can draw conclusions about the size range of the collected particles. Figure 14 shows the simulated capture zenith angle with particle radius assuming the reference β-curve and a density of 2 g cm^{-3}. From this curve, we conclude that particles with radii smaller than about 0.25 μm will not be captured by Stardust: either they are not present because of the position of Stardust

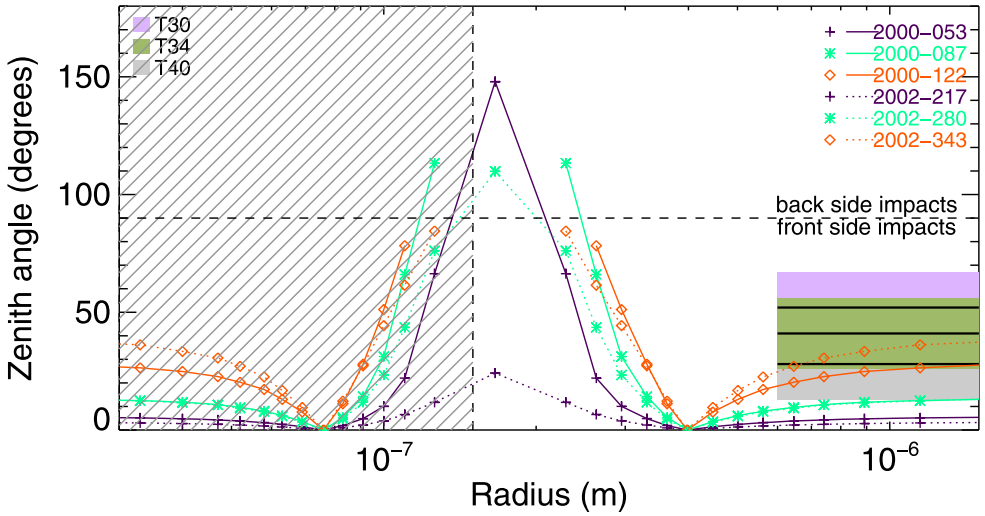

Fig. 14. The zenith angle of the ISD impact direction on the Stardust collector plotted against increasing particle radius a is shown for six epochs during the two collection periods (labeled as "year – day-of-year"). For this graph, the reference β-curve and a particle density of 2 g cm^{-3} was assumed. The boxes indicate the range of radii of the three ISD candidates given by Westphal et al. (2014) and Butterworth et al. (2014). The color labels T30, T34, and T40 correspond to tracks 30, 34, and 40 (Westphal et al. 2014), respectively. Lorentz forces are not taken into account in this plot. Therefore, the hatched region denotes the radii of particles of which large or total filtering is expected (see also Fig. 6 and Table 2).

with respect to the β-cones, or they will impact on the cometary side of the dust collector (zenith angles > 90°), or they are filtered out by Lorentz forces (hatched region in Fig. 14 and earlier discussions). The only period in which also the smallest particles (if not filtered by Lorentz forces) could have been captured with the ISD-side of the collector is the beginning of the second collection period (cf. the purple dotted line in Fig. 14). The boxes in Fig. 14 indicate the range of radii of two particles given by Westphal et al. (2014) and Butterworth et al. (2014).

Particle Properties

By comparing the estimated velocities of the three contemporary ISD candidates from Postberg et al. (2014) to the results of the simulations, we could constrain the range of β-values for these captured particles to be between 1.0 and 1.6 for tracks 30 and 34 and between 0 and 1 for track 40. The β-value depends on size, material, and structure of the particle, where the size is the most determining parameter: very large and very small particles generally have low β-values (thus, particles of the same material will still have different β-values according to their size). However, the masses and sizes as reported in Butterworth et al. (2014) and Westphal et al. (2014) are fairly large (3.1 and 4.4 pg for tracks 30 and 34 with diameters above 1 μm), which suggests that they are larger optical cross sections and/or have lower densities to have high β-values.

In Fig. 14, we plotted the impact zenith angle with particle radius assuming the reference β-curve and a density of 2 g cm^{-3}. The zenith angle of track 40 matches the expected value of ISD grains for the observed particle mass, whereas the zenith angles of tracks 30 and 34 are higher than the expected values for the observed masses. In summary, not all of the measured four parameters (particles mass, impact speed, azimuth, and zenith angles) seem to fit the values expected from modeling for all particles. In the following, we will discuss the effects of a variation in the assumed particle properties and, hence, a variation in the assumed β-curve.

Particles that are porous, fractal, or fluffy will have a different β-curve than assumed here, and thus the lower and upper size limit of simulated particles that could be captured (like shown in Fig. 14) will differ. Particles with similar optical properties but lower density generally have a higher β-value for the same size as they have a higher cross section per mass and thus experience more solar radiation pressure force (Schwehm 1976; Gustafson 1994). However, if the particles have a fractal-like structure, their β-values would be lower (Mukai et al. 1992; Kimura and Mann 1999). This means that high β-values as found for tracks 30 and 34 would either point at particles, which are (very) low in density (possibility A), or at smaller particles (in the $\beta > 1$ region of the β-curve) of different composition than the original astronomical silicates from Draine and Lee (1984) and Gustafson (1994) (possibility B, although the masses and sizes found for

the three candidates were rather large) or a compromise between these two (possibility C): semiporous particles with different optical properties than the compact silicates. Core-mantle particles (Li and Greenberg 1997) could be an example of these. Their β-values correspond well to the Ulysses measurements (Kimura et al. 2003) and it is not implausible that they may lose their mantle upon impact in aerogel. From the Stardust ISD impact velocities and the simulations alone, we cannot infer why these β-values are high without information on the optical properties of local LIC particles, but the velocities, simulation results, and exact sizes of the original particles could possibly confirm more porous structures. In principle, this question thus remains open (depending on uncertainties in the size determination of the original impacting particle), but the low bulk densities that were found in tracks 30 and 34 (Butterworth et al. 2014; Westphal et al. 2014) suggest that the particles are indeed porous to some extent. The high β-values found here correspond well to the findings of Landgraf et al. (1999a) who stated that β_{max} of the local ISD is between 1.4 and 1.8. Although the low densities as reported in Butterworth et al. (2014) strongly point toward scenario A, the fact that the particles survived the impact intact rather points to scenarios B and C (although scenario B is not probable because of the large sizes of the residual grains). The charge-to-mass ratio of porous particles or other nonspherical particles is higher than for compact spheres (Ma et al. 2012) meaning that bigger particles would be filtered out even more easily than assumed in this study and than shown in Table 2.

CONCLUSIONS AND OUTLOOK

We simulated the impact speeds and directions onto the Stardust collector for the two collection periods of the Stardust mission and compared the preliminary results of the ISPE to these simulations. The simulation included solar gravity and solar radiation pressure force and for the flux calculations also included Lorentz forces. The bases for the simulation were dynamical parameters of the interstellar dust flow as determined by Ulysses. The parameters include the incoming flow direction of 259° ecliptic longitude and 8° ecliptic latitude, the β-curve for astrosilicates from Gustafson (1994) with a maximum β of 1.6, and a charge-to-mass ratio Q/m corresponding to a surface potential of +5 V for spherical particles of density $\rho = 2$ g cm^{-3}. For calculating the Lorentz forces, we took into account the time-varying solar wind magnetic field as described by the Parker spiral. With these assumptions, we calculated for differently sized particles the impact speeds and directions onto the Stardust collector for several times during the two collection periods of the Stardust mission. A range of impact directions (zenith angle and azimuth) and speeds (3–25 km s^{-1}) was determined for particles of different radii (0.2–2 μm) during the two collection periods.

Stardust was exposed to the interstellar dust stream just after the solar minimum of the "defocusing" phase of the solar cycle where the defocusing effect of the Lorentz force is prominent. The Lorentz force filters out all particles smaller than about 0.15 μm, and severely reduces the particle density for particles smaller than 0.25 μm. For bigger particles, the Lorentz force does not play a large role in the impact velocity and direction calculations for Stardust during the collection period. Therefore, the main parameters influencing the results are density and the beta curve.

Particles with radii between 0.25 and 0.4 μm have predicted impact speeds between 3 and 14 km s^{-1}, particles between 0.4 and 0.7 μm have impact speeds between 10 and 20 km s^{-1}, and particles larger than 0.7 μm have impact speeds between 14 and 25 km s^{-1}. The ISD zenith angles are mostly within 40° from the collector normal for particles with impact speeds >10 km s^{-1} (not taking into account the spacecraft pointing uncertainty). The zenith angles increase for particles with impact speeds below 10 km s^{-1} and even become >90°. Such particles would impact on the cometary side of the collector. The simulated azimuth angles on the collector concentrate around 0° for particles with high impact velocity (the largest particles) and around 180° for the particles with slower impact velocities.

The expected number of collected particles by Stardust was calculated based on the measurements of ISD made by the Ulysses spacecraft. This was done using our simulation tool including the Lorentz force and calculating the flux of ISD particles at the heliospheric boundary that provides the filtered flux at Ulysses' position and time. This flux was then filtered to the position and times of Stardust collection periods. We predict for the Stardust collection a total of 50 ISD particles of density $\rho = 2$ g cm^{-3}.

Particle properties, like the density (porosity or fluffiness), will have an influence on the velocities and directions because they would have a slightly different β-curve than assumed here. In addition, a lower density will lower the estimated amount of captured particles because of the higher charge-to-mass ratio and thus more filtering by Lorentz forces for the less massive particles.

Up to now, three ISD candidates have been identified in the aerogel tiles by the ISPE Team. Four more craters were found in the foils (Stroud et al. 2012). The particle radii are limited to particles larger than approximately 0.25 μm and approximately 30% of

the surface has been analyzed. It is expected that more candidates will be found. From analyses of the tracks and particle residues in the tracks, the ISPE Team determined the impact directions and estimated the impact speeds.

The measured zenith angles and speeds of the three ISD candidates correspond well to the calculated impact speeds and zenith angles of dust with β-value between 1.0 and 1.5 (tracks 30 and 34) and the particle of track 40 must have had $\beta < 1$. The azimuth angle of one candidate particle is compatible with the simulated azimuth angle, but for two others, the measured angle deviates significantly from the predicted angles for ISD particles with the assumed dynamical parameters. However, by tuning these assumptions, a compatible solution can be found to match the observed particles with the simulations: another particle density and a shifted initial dust direction (274°) could probably make all three particles correspond to the observed azimuth angles, zenith angles, impact speeds, and particle sizes.

We conclude that the trajectories and capture speeds are consistent with the propagation model within its uncertainties and assumptions. The main uncertainties are spacecraft pointing, particle density, particle material (β-curve), initial ISD speed and direction, and uncertainties in measured speed and direction of the extracted particle candidates. Another uncertainty comes from not knowing "when" the particle has impacted and thus what the relative velocity of the particle with respect to the spacecraft was. Because the trajectories are sensitive to small changes in ISD radiant longitude (Frank et al. 2013; Westphal et al. 2014), mainly along the sunward-antisunward direction, a significant reduction in the uncertainty in the radiant longitude direction could provide a significantly improved test of interstellar origin (Fig. 9). Nevertheless, the only known alternative to an interstellar origin is an interplanetary origin, which is expected to show a quite different distribution to that observed (Frank et al. 2013), even within the very limited statistics. The small number of the identified particles and the uncertainties of the dynamical characteristics prevent constraining dynamical interstellar dust properties at the present time. When more interstellar particles are identified in the Stardust collector, the ISD dynamical properties and the ISD flow may be further constrained.

Recently, improved instrumentation has been developed and tested that will reduce many of the uncertainties Stardust was facing. A novel active cosmic dust collector (Grün et al. 2012) consisting of a dust trajectory sensor in combination with particle collectors like those used in the Stardust mission has been developed and tested at a dust accelerator. The dust trajectory sensor determines the trajectories of electrically charged particles, via the induced charge onto an array of sensor electrodes before they impact into the collector material. The instrument provides trajectory measurement with accuracy better than 1% in speed and 1° in directionality for micrometer and submicrometer-sized particles, depending on the charge signal-to-noise ratio. Application of an active cosmic dust collector for collection of interplanetary and interstellar dust particles at 1 AU will be possible at the corresponding fluxes. For each collected particle, the impact position will be known to sub-mm accuracy, which significantly eases the task of locating the particle on the collector material. In addition, the velocity vector and impact time will be recorded. The accuracy of the velocity vector will be sufficient to distinguish interstellar from interplanetary particles. Dedicated sample return missions like Stardust 2 or SARIM (Srama et al. 2009, 2012) equipped with active cosmic dust collectors will open new avenues in interplanetary and interstellar dust research.

Acknowledgments—We thank the reviewers and the AE Christian Koeberl, for their thoughtful reviews that greatly improved this manuscript. We also thank the AE John Bradley for his critical input and time and effort spent reviewing the ISPE manuscripts. The ISPE consortium gratefully acknowledge the NASA Discovery Program for Stardust, the fourth NASA Discovery mission. AJW, ALB, ZG, RL, DZ, WM, and JVK were supported by NASA grant NNX09AC36G. RMS, HCG, and NDB were supported by NASA grant NNH11AQ61I. VJS acknowledges support from ESA. The Advanced Light Source is supported by the Director, Office of Science, Office of Basic Energy Sciences, of the U.S. Department of Energy under Contract No. DE-AC02-05CH11231. Use of the National Synchrotron Light Source, Brookhaven National Laboratory, was supported by the U.S. Department of Energy, Office of Science, Office of Basic Energy Sciences, under Contract No. DE-AC02-98CH10886.

Editorial Handling—Dr. Christian Koeberl

REFERENCES

Brownlee D. E., Tsou P., Aléon J., Alexander C. M. O'D., Araki T., Bajt S., Baratta G. A., Bastien R., Bland P., Bleuet P., Borg J., Bradley J. P., Brearley A., Brenker F., Brennan S., Bridges J. C., Browning N. D., Brucato J. R., Bullock E., Burchell M. J., Busemann H., Butterworth A., Chaussidon M., Cheuvront A., Chi M., Cintala M. J., Clark B. C., Clemett S. J., Cody G., Colangeli L., Cooper G., Cordier P., Daghlian C., Dai Z., D'Hendecourt L., Djouadi Z., Dominguez G., Duxbury T., Dworkin J. P., Ebel D. S., Economou T. E., Fakra S., Fairey S. A. J., Fallon S., Ferrini G., Ferroir T., Fleckenstein H., Floss C., Flynn G.,

Franchi I. A., Fries M., Gainsforth Z., Gallien J.-P., Genge M., Gilles M. K., Gillet P., Gilmour J., Glavin D. P., Gounelle M., Grady M. M., Graham G. A., Grant P. G., Green S. F., Grossemy F., Grossman L., Grossman J. N., Guan Y., Hagiya K., Harvey R., Heck P., Herzog G. F., Hoppe P., Hörz F., Huth J., Hutcheon I. D., Ignatyev K., Ishii H., Ito M., Jacob D., Jacobsen C., Jacobsen S., Jones S., Joswiak D., Jurewicz A., Kearsley A. T., Keller L. P., Khodja H., Kilcoyne A. L. D., Kissel J., Krot A., Langenhorst F., Lanzirotti A., Le L., Leshin L. A., Leitner J., Lemelle L., Leroux H., Liu M.-C., Luening K., Lyon I., MacPherson G., Marcus M. A., Marhas K., Marty B., Matrajt G., McKeegan K., Meibom A., Mennella V., Messenger K., Messenger S., Mikouchi T., Mostefaoui S., Nakamura T., Nakano T., Newville M., Nittler L. R., Ohnishi I., Ohsumi K., Okudaira K., Papanastassiou D. A., Palma R., Palumbo M. E., Pepin R. O., Perkins D., Perronnet M., Pianetta P., Rao W., Rietmeijer F. J. M., Robert F., Rost D., Rotundi A., Ryan R., Sandford S. A., Schwandt C. S., See T. H., Schlutter D., Sheffield-Parker J., Simionovici A., Simon S., Sitnitsky I., Snead C. J., Spencer M. K., Stadermann F. J., Steele A., Stephan T., Stroud R., Susini J., Sutton S. R., Suzuki Y., Taheri M., Taylor S., Teslich N., Tomeoka K., Tomioka N., Toppani A., Trigo-Rodrguez J. M., Troadec D., Tsuchiyama A., Tuzzolino A. J., Tyliszczak T., Uesugi K., Velbel M., Vellenga J., Vicenzi E., Vincze L., Warren J., Weber I., Weisberg M., Westphal A. J., Wirick S., Wooden D., Wopenka B., Wozniakiewicz P., Wright I., Yabuta H., Yano H., Young E. D., Zare R. N., Zega T., Ziegler K., Zimmerman L., Zinner E., and Zolensky M. 2006. Comet 81P/Wild 2 under a microscope. *Science* 314:1711–1716.

Burchell M. J., Thomson R., and Yano H. 1998. Capture of hypervelocity particles in aerogel: In ground laboratory and low earth orbit. *Planetary and Space Science* 47:189–204.

Burchell M. J., Cole M. J., Price M. C., and Kearsley A. T. 2012. Experimental investigation of impacts by solar cell secondary ejecta on silica aerogel and aluminum foil: Implications for the Stardust Interstellar Dust Collector. *Meteoritics & Planetary Science* 47:671–683.

Butterworth A. L., Westphal A. J., Tyliszczak T., Gainsforth Z., Stodolna J., Frank D., Allen C., Anderson D., Ansari A., Bajt S., Bastien R. S., Bassim N., Bechtel H. A., Borg J., Brenker F. E., Bridges J., Brownlee D. E., Burchell M., Burghammer M., Changela H., Cloetens P., Davis A. M., Doll R., Floss C., Flynn G., Grün E., Heck P. R., Hillier J. K., Hoppe P., Hudson B., Huth J., Hvide B., Kearsley A., King A. J., Lai B., Leitner J., Lemelle L., Leroux H., Leonard A., Lettieri R., Marchant W., Nittler L. R., Ogliore R., Ong W. J., Postberg F., Price M. C., Sandford S. A., Sans Tresseras J., Schmitz S., Schoonjans T., Silversmit G., Simionovici A., Solé V. A., Srama R., Stadermann F., Stephan T., Sterken V., Stroud R. M., Sutton S., Trieloff M., Tsou P., Tsuchiyama A., Vekemans B., Vincze L., Korff J. V., Wordsworth N., Zevin D., Zolensky M. E., and > 30,000 Stardust@home dusters. 2014. Stardust Interstellar Preliminary Examination IV: Scanning transmission X-ray microscopy analyses of impact features in the Stardust Interstellar Dust Collector. *Meteoritics & Planetary Science*, doi:10.1111/maps.12220.

Draine B. T. and Lee H. M. 1984. Optical properties of interstellar graphite and silicate grains. *The Astrophysical Journal* 285:89–108.

Frank D., Westphal A. J., Zolensky M. E., Gainsforth Z., Bastien R. S., Allen C., Anderson D., Ansari A., Bajt S., Bassim N., Bechtel H. A., Borg J., Brenker F. E., Bridges J., Brownlee D. E., Burchell M., Burghammer M., Butterworth A. L., Changela H., Cloetens P., Davis A. M., Doll R., Floss C., Flynn G., Grün E., Heck P. R., Hillier J. K., Hoppe P., Hudson B., Huth J., Hvide B., Kearsley A., King A. J., Lai B., Leitner J., Lemelle L., Leroux H., Leonard A., Lettieri R., Marchant W., Nittler L. R., Ogliore R., Ong W. J., Postberg F., Price M. C., Sandford S. A., Tresseras J. S., Schmitz S., Schoonjans T., Silversmit G., Simionovici A., Solé V. A., Srama R., Stephan T., Sterken V., Stodolna J., Stroud R. M., Sutton S., Trieloff M., Tsou P., Tsuchiyama A., Tyliszczak T., Vekemans B., Vincze L., Korff J. V., Wordsworth N., Zevin D., and > 30,000 Stardust@home dusters. 2013. Stardust Interstellar Preliminary Examination II: Curating the interstellar dust collector, picokeystones, and sources of impact tracks. *Meteoritics & Planetary Science*, doi:10.1111/maps.12147.

Frisch P. C., Dorschner J. M., Geiss J., Greenberg J. M., Grün E., Landgraf M., Hoppe P., Jones A. P., Krätschmer W., Wolfgang L., Timur J., Morfill G. E., Reach W., Slavin J. D., Svestka J., Witt A. N., and Zank Gary P. 1999. Dust in the local interstellar wind. *The Astrophysical Journal* 525:492–516.

Grün E., Zook H. A., Baguhl M., Balogh A., Bame S. J., Fechtig H., Forsyth R., Hanner M. S., Horanyi M., Kissel J., Lindblad B.-A., Linkert D., Linkert G., Mann I., McDonnell J. A. M., Morfill G. E., Phillips J. L., Polanskey C., Schwehm G., Siddique N., Staubach P., Svestka J., and Taylor A. 1993. Discovery of Jovian dust streams and interstellar grains by the ULYSSES spacecraft. *Nature* 362:428–430.

Grün E., Sternovsky Z., Horanyi M., Hoxie V., Robertson S., Xi J., Auer S., Landgraf M., Postberg F., Price M. C., Srama R., Starkey N. A., Hillier J. K., Franchi I. A., Tsou P., Westphal A., and Gainsforth Z. 2012. Active cosmic dust collector. *Planetary and Space Science* 60:261–273.

Gustafson B. S. 1994. Physics of zodiacal dust. *Annual Review of Earth and Planetary Sciences* 22:553–595.

Kempf S., Srama R., Altobelli N., Auer S., Tschernjawski V., Bradley J., Burton M. E., Helfert S., Johnson T. V., Krüger H., Moragas-Klostermeyer G., and Grün E. 2004. Cassini between Earth and asteroid belt: First in-situ charge measurements of interplanetary grains. *Icarus* 171:317–335.

Kimura H. and Mann I. 1999. Radiation pressure on porous micrometeoroids, Meteoroids 1998, Proceedings of the International Conference held at Tatranska Lomnica, Slovakia, August 17–21, 1998, edited by Baggaley W. J. and Porubcan. V. Astronomical Institute of the Slovak Academy of Sciences. p. 283.

Kimura H., Okamoto H., and Mukai T. 2002. Radiation pressure and the poynting-robertson effect for fluffy dust particles. *Icarus* 157:349–361.

Kimura H., Mann I., and Jessberger E. K. 2003. Composition, structure, and size distribution of dust in the local interstellar cloud. *The Astrophysical Journal* 583:314–321.

Landgraf M. 1998. Modellierung der Dynamik und Interpretation der In-Situ Messung interstellaren Staubs in der Lokalen Umgebung des Sonnensystems. Ph.D. thesis, Ruprecht-Karls-Universität Heidelberg, Germany.

Landgraf M., Augustsson K., Grün E., and Gustafson B. Å. S. 1999a. Deflection of the local interstellar dust flow by solar radiation pressure. *Science* 286:2319–2322.

Landgraf M., Müller M., and Grün E. 1999b. Prediction of the in-situ dust measurements of the Stardust mission to comet 81P/Wild 2. *Planetary and Space Science* 47:1029–1050.

Landgraf M., Baggaley W. J., Grün E., Krüger H., and Linkert G. 2000. Aspects of the mass distribution of interstellar dust grains in the solar system from in situ measurements. *Journal of Geophysical Research* 105:10343–10352.

Landgraf M., Krüger H., Altobelli N., and Grün E. 2003. Penetration of the heliosphere by the interstellar dust stream during solar maximum. *Journal of Geophysical Research* 108(A10):LIS 5-1.

Li A. and Greenberg J. M. 1997. A unified model of interstellar dust. *Astronomy & Astrophysics* 323:566–584.

Linde T. J. and Gombosi T. I. 2000. Interstellar dust filtration at the heliospheric interface. *Journal of Geophysical Research* 105:10411–10418.

Linsky J. L., Rickett B. J., and Redfield S. 2008. The origin of radio scintillation in the local interstellar medium. *The Astrophysical Journal* 675:413–419.

Ma Q., Matthews L., Land V., and Hyde T. 2012. Charging of aggregate grains in astrophysical environments. *The Astrophysical Journal* 763:77–86.

Mathis J. S., Rumpl W., and Nordsieck K. H. 1977. The size distribution of interstellar grains. *The Astrophysical Journal* 217:425–433.

McComas D. J., Alexashov D., Bzowski M., Fahr H., Heerikhuisen J., Izmodenov V., Lee M. A., Möbius E., Pogorelov N., Schwadron N. A., and Zank G. P. 2012. The heliosphere's interstellar interaction: No bow shock. *Science* 336:1291–1293.

Mukai T., Ishimoto H., Kozasa T., Blum J., and Greenberg J. M. 1992. Radiation pressure forces of fluffy porous grains. *Astronomy & Astrophysics* 262:315–320.

Postberg F., Hillier J. K., Armes S. P., Bugiel S., Butterworth A. L., Dupin D., Fielding L. A., Fujii S., Gainsforth Z., Grün E., Li Y. W., Srama R., Sterken V., Stodolna J., Trieloff M., Westphal A. J., Allen C., Anderson D., Ansari A., Bajt S., Bastien R. S., Bassim N., Bechtel H. A., Borg J., Brenker F. E., Bridges J., Brownlee D. E., Burchell M., Burghammer M., Changela H., Cloetens P., Davis A. M., Doll R., Floss C., Flynn G., Frank D., Heck P. R., Hoppe P., Hudson B., Huth J., Hvide B., Kearsley A., King A. J., Lai B., Leitner J., Lemelle L., Leroux H., Leonard A., Lettieri R., Marchant W., Nittler L. R., Ogliore R., Ong W. J., Price M. C., Sandford S. A., Tresseras J. S., Schmitz S., Schoonjans T., Silversmit G., Simionovici A., Solé V. A., Stadermann F., Stephan T., Stroud R. M., Sutton S., Tsou P., Tsuchiyama A., Tyliszczak T., Vekemans B., Vincze L., Korff J. V., Wordsworth N., Zevin D., Zolensky M. E., and > 30,000 Stardust@home dusters. 2014. Stardust Interstellar Preliminary Examination IX: High speed interstellar dust analogue capture in Stardust flight-spare aerogel. *Meteoritics & Planetary Science*, doi:10.1111/maps.12173.

Schwehm G. 1976. Radiation pressure on interplanetary dust particles. In *Lecture notes in physics, Vol. 48, Interplanetary dust and zodiacal light*, edited by Elsaesser H. and Fechtig H. Berlin: Springer Verlag. pp. 459–463.

Slavin J. D., Frisch P. C., Heerikhuisen J., Pogorelov N. V., Mueller H.-R., Reach W. T., Zank G. P., Dasgupta B., and Avinash K. 2010. Exclusion of tiny interstellar dust grains from the heliosphere. *Twelfth International Solar Wind Conference, AIP Conference Proceedings* 1216:497–501.

Slavin J. D., Frisch P. C., Müller H.-R., Heerikhuisen J., Pogorelov N. V., Reach W. T., and Zank G. 2012. Trajectories and distribution of interstellar dust grains in the heliosphere. *The Astrophysical Journal* 760:46–61.

Srama R., Stephan T., Grün E., Pailer N., Kearsley A., Graps A., Laufer R., Ehrenfreund P., Altobelli N., Altwegg K., Auer S., Baggaley J., Burchell M. J., Carpenter J., Colangeli L., Esposito F., Green S. F., Henkel H., Horanyi M., Jäckel A., Kempf S., McBride N., Moragas-Klostermeyer G., Krüger H., Palumbo P., Srowig A., Trieloff M., Tsou P., Sternovsky Z., Zeile O., and Röser H.-P. 2009. Sample return of interstellar matter (SARIM). *Experimental Astronomy* 23:303–328.

Srama R., Krüger H., Yamaguchi T., Stephan T., Burchell M., Kearsley A. T., Sterken V., Postberg F., Kempf S., Grün E., Altobelli N., Ehrenfreund P., Dikarev V., Horanyi M., Sternovsky Z., Carpenter J. D., Westphal A., Gainsforth Z., Krabbe A., Agarwal J., Yano H., Blum J., Henkel H., Hillier J., Hoppe P., Trieloff M., Hsu S., Mocker A., Fiege K., Green S. F., Bischoff A., Esposito F., Laufer R., Hyde T. W., Herdrich G., Fasoulas S., Jäckel A., Jones G., Jenniskens P., Khalisi E., Moragas-Klostermeyer G., Spahn F., Keller H. U., Frisch P., Levasseur-Regourd A. C., Pailer N., Altwegg K., Engrand C., Auer S., Silen J., Sasaki S., Kobayashi M., Schmidt J., Kissel J., Marty B., Michel P., Palumbo P., Vaisberg O., Baggaley J., Rotundi A., and Röser H. P. 2012. SARIM PLUS sample return of comet 67P/CG and of interstellar matter. *Experimental Astronomy* 33:723–751.

Sterken V. J., Altobelli N., Kempf S., Krüger H., Srama R., Strub P., and Grün E. 2012a. The filtering of interstellar dust in the solar system. *Astronomy & Astrophysics* 552 (A130):22.

Sterken V. J., Altobelli N., Kempf S., Schwehm G., Srama R., and Grün E. 2012b. The flow of interstellar dust into the solar system. *Astronomy & Astrophysics* 538(A102):24.

Stroud R. M., Allen C., Anderson D., Ansari A., Bajt S., Bassim N., Bastien R. S., Bechtel H. A., Borg J., Brenker F. E., Bridges J., Brownlee D. E., Burchell M., Burghammer M., Butterworth A. L., Changela H., Cloetens P., Davis A. M., Doll R., Floss C., Flynn G., Frank D., Gainsforth Z., Grün E., Heck P. R., Hillier J. K., Hoppe P., Huth J., Hvide B., Kearsley A., King A. J., Lai B., Leitner J., Lemelle L., Leroux H., Leonard A., Lettieri R., Marchant W., Nittler L. R., Ogliore R., Ong W. J., Postberg F., Price M. C., Sandford S. A., Sans Tresseras J., Schmitz S., Schoonjans T., Silversmit G., Simionovici A., Solé V. A., Srama R., Stephan T., Sterken V., Stodolna J., Sutton S., Trieloff M., Tsou P., Tsuchiyama A., Tyliszczak T., Vekemans B., Vincze L., Korff J. V., Westphal A. J., Zevin D., Zolensky M. E., and > 30,000 Stardust@home dusters. 2014. Stardust Interstellar Preliminary Examination XI: Identification and elemental analysis of impact craters on Al foils from the Stardust Interstellar Dust Collector. *Meteoritics & Planetary Science*, doi:10.1111/maps.12136.

Tsou P., Brownlee D. E., Sandford S. A., Horz F., and Zolensky M. E. 2003. Wild 2 and interstellar sample collection and Earth return. *Journal of Geophysical Research—Planets* 108:8113 (21 p).

Westphal A. J., Zolensky M. E., Gainsforth Z., Bastien R. S., Allen C., Anderson D., Ansari A., Bajt S., Bassim N., Bechtel H. A., Borg J., Brenker F. E., Bridges J., Brownlee D. E., Burchell M., Burghammer M., Butterworth A. L., Changela H., Cloetens P., Davis A. M., Doll R., Floss C., Flynn G., Frank D., Grün E., Heck P. R., Hillier J. K., Hoppe P., Hudson B., Huth J., Hvide B., Kearsley A., King A. J., Lai B., Leitner J., Lemelle L., Leroux H., Leonard A., Lettieri R., Marchant W., Nittler L. R., Ogliore R., Ong W. J., Postberg F., Price M. C., Sandford S. A., Tresseras J. S., Schmitz S., Schoonjans T., Silversmit G., Simionovici A., Solé V. A., Srama R., Stadermann F., Stephan T., Sterken V., Stodolna J., Stroud R. M., Sutton S., Trieloff M., Tsou P., Tsuchiyama A., Tyliszczak T., Vekemans B., Vincze L., Korff J. V., Wordsworth N., Zevin D., and >30,000 Stardust@home dusters. 2014. Final reports of the Stardust Interstellar Preliminary Examination. *Meteoritics & Planetary Science*, doi:10.1111/maps.12221.

Witte M., Rosenbauer H., Banaszkiewicz M., and Fahr H. 1993. The ULYSSES neutral gas experiment—Determination of the velocity and temperature of the interstellar neutral helium. *Advances in Space Research* 13:121–130.